Influence of nonmetallic elements doping on the NH_3-SCR activity and properties of $Ce_{20}W_{10}Ti_{100}O_z$ catalyst via melamine modification

Zhibo Xiong[1], Jiaxing Liu[1], Fucheng Guo[1], Yanping Du[2], Fei Zhou[1,3], Qiguo Yang[1]*, Wei Lu[1], Huancong Shi[4,5]**

1. School of Energy and Power Engineering, University of Shanghai for Science & Technology, Shanghai, 200093, China

2. Department of Engineering, Faculty of Environment, Science and Economy, University of Exeter, Penryn Campus, Penryn, Cornwall TR109FE, UK

3. Jiangsu Guoxin Jingjiang Power Generation Co., Ltd., Jingjiang, 214500, China

4. Huzhou Institute of Zhejiang University, Huzhou, Zhejiang Province, 313000, China

5. Zhejiang University, Hangzhou, Zhejiang Province, 310058, China

Abstract: In this study, the melamine (Mel) modification method was adopted to optimize the NH_3-SCR activity of $Ce_{20}W_{10}Ti_{100}O_z$ doped with C or/and N elements. It was found that with the improved doping of C or/and N into the lattice of anatase TiO_2 of $Ce_{20}W_{10}Ti_{100}O_z$, the dispersion of tungsten/cerium species and the conversion of partial Ce^{4+} to Ce^{3+} on its surface were significant enhanced, resulting in a large improvement of its surface chemical adsorbed oxygen(O_α) concentration. Interestingly, the enhancement of Mel/$Ti(SO_4)_2$ mass ratio slightly decreases the surface N/O_α concentrations, but further improves the surface Ti concentration and $Ce^{3+}/(Ce^{3+}+Ce^{4+})$ molar ratio. Furthermore, Mel modification increases the surface/sub-surface oxygen relative concentrations of $Ce_{20}W_{10}Ti_{100}O_z$, although decreases its low-temperature reducibility and acidity. Due to the larger N doped amount, $Ce_{20}W_{10}Ti_{100}O_z$-Mel$_t$:Ti=1:2 shows a higher surface acidity and $O_\alpha/(O_\alpha+O_\beta)$ molar ratio than $Ce_{20}W_{10}Ti_{100}O_z$-Mel$_t$:Ti=4:2, which might be responsible for its

* Corresponding author: Qiguo Yang, Tel.: +86 21 55272320

** Corresponding author. Huancong Shi, Email addresses: yangqg@usst.edu.cn (Q. Yang), hcshi@usst.edu.cn (H. Shi).

improved catalytic performance due to the melamine (Mel) modification.

Keywords: NH_3-SCR, Nonmetallic elements doping, Melamine modification, Surface composition

1. Introduction

In recent years, accompanying the rapid process of industrialization and civilization, the emission of nitrogen oxides (NO_x) from fossil fuel and automobile inevitably causes environmental issues, such as photochemical smog, acid rain, ozone depletion and greenhouse effect [1,2]. Nowadays, selective catalytic reduction of NO_x with NH_3 (NH_3-SCR) is an efficient method to control NO_x with V_2O_5-WO_3(MoO_3)/TiO_2 as the commercial catalyst due to its high efficiency and excellent hydrothermal stability [3-5]. Meanwhile, there exists some unavoidable problems which restrict the practical applications of the commercial catalyst, including the narrow temperature range of 300～400 °C, the high conversion of SO_2 to SO_3 and the poison of vanadium pentoxide to human health and environment [6,7]. Accordingly, it is desirable to develop novel NH_3-SCR catalyst to substitute the conventional V_2O_5-WO_3(MoO_3)/TiO_2 catalyst [2,8,9].

At present, various types of metal oxide catalysts, using copper, titanium, iron, manganese, nickel and cerium as the basic active components, have been studied and developed in photocatalysis [10-15], electrocatalytic [16-18], NO_x reduction [19,20] and other fields [21,22] due to the good crystal structure and magnetic structure characteristics [23-26]. Hassan et al. prepared a series of Se-doped $NiFe_2O_4$ and found that the introduction of Se led better conductivity of $NiFe_2O_4$ and makes it easier for electrons to transfer from the electrode to the catalyst surface. In addition, the addition of selenium provided more surface area and active sites to the decomposition of water [18]. Anantharaman et al had reported that the perovskite phase

Cerium Titanium Ferrites ($CeTi_{1-x}Fe_xO_{3-\delta}$) nanocatalyst had smaller grain size, more oxygen vacancies and higher magnetic saturation, thus presented the prosperous photocatalytic performance [27]. Xu et al. confirmed that the introduction of an appropriate amount of TiO_2 could effectively improve the NH_3-SCR performance of $WO_3/CeZrTi_xO_2$ series catalysts. In addition, the addition of TiO_2 promoted the adsorption and activation of NH_3 and increased the reactivity of adsorbed nitrate species with NH_3 species, which significantly affected the NH_3-SCR performance [28]. Therefore, nano metal oxide catalysts with metal elements as the main active components have attracted wide attention.

Among them, cerium oxide (CeO_2) has received much attention in NH_3-SCR reaction due to its remarkable oxygen storage capacity, high Ce^{3+}/Ce^{4+} conversion and outstanding reducibility property [29-31]. Meanwhile, owing to the unselective oxidation of NH_3 at high temperatures and the lack of acid sites, single CeO_2 presents a low activity in NH_3-SCR reaction. The combination of different compounds could generate new composite materials with excellent electronic and structural properties, and the addition of other metal elements help to enhance the acidity or/and the oxygen vacancy of cerium oxide, significantly improves the electronic properties of the obtained composites [32-34], thereby increases its NH_3-SCR activity, for instance W [35], Fe [36], Cu [37], Ni [38]. When titanium is doped into other metals, it can occupy the non-equivalent crystal position and affect the crystal structure parameters, thus make the resistivity and the temperature of transition to the activated conductivity [25,39]. Besides, owing to the nontoxicity, chemical inertness, stability and effectiveness, TiO_2 is commonly used as the carrier of cerium-based catalyst in the NH_3-SCR reaction. Therefore, CeO_2/TiO_2 has received great attention in the field of NH_3-SCR reaction. It had been proven that CeO_2/TiO_2 exhibited excellent

medium-temperature NH_3-SCR activity. Meanwhile, this catalyst showed poor anti-poisoning under the high-concentration of SO_2 [40,41]. Thus, other additives were also introduced to further enhance the NH_3-SCR activity and anti-SO_2 poisoning of CeO_2/TiO_2 via the synergistic effect of components [42], for example, Cu [43], Mo [44], Mn [45] or W [46] et al. The W-based composites exhibit excellent electrical, mechanical and thermal properties and the introduction of WO_3 could enhance the concentrations of the active oxygen species and acid sites through the synergistic effect of cerium and titanium components, thereby significantly improved the NH_3-SCR activity of cerium-titanium mixed oxide catalyst [47-49]. Park et al. found that the tungsten-doped $CeTiO_x$ catalyst could achieve 100% NO_x conversion at 250～400 °C due to the enhancement of tungsten-doping on its oxygen vacancy and reduction properties [50]. Thus, cerium-tungsten-titanium mixed oxide is a suitable replacement for the conventional V_2O_5-$WO_3(MoO_3)/TiO_2$ catalyst owing to the excellent NH_3-SCR activity.

The previous studies had pointed out that the preparation methods affected the morphologies crystal structures, mechanical and optical properties of the composite metal oxides, thus had a greater impact on the physical and chemical properties of catalysts [51-53]. It has been reported that when Ni-Fe thin films were deposited on silicon substrates by electrodeposition, the average crystal size of the growth was less than the critical value (10 nm), which could provide less roughness, defects and greater thickness of the film uniformity [54]. The synthesized TiO_2 via the improved hydrothermal homogeneous precipitation method contributed to increasing the reduction of NO_x to 94.12%, and the hydrothermal treatment significantly improved the specific surface area, particle size and uniformity of TiO_2 samples [55]. Furthermore, our previous research also confirmed that $Ce_{20}W_{10}Ti_{100}O_z$ synthesized via one-pot hydrothermal co-precipitation presented a better NH_3-SCR

activity [56].

Interestingly, the doping of nonmetallic elements has also been confirmed to improve the activity of metal oxide-based catalysts by inducing the surface structural defects/oxygen vacancies and changing the electronic properties [57-60]. Zeng et al. found that the doping of phosphorus inhibited the agglomeration of TiO_2 and promoted the dispersion of CeO_2 on the surface of CeO_2/TiO_2, thereby enhanced its NH_3-SCR activity [61]. Liu et al. had investigated the influence of sulfur-doping on the NO_x reduction of MnO_x/TiO_2, and found that the doping of S contributed to bringing the distortion of TiO_2 lattice, thereby improved the acidity and redox property of catalyst [58]. Cong et al. reported that the doping of nitrogen enriched the Brønsted acid sites of ceria oxide and inhibited the oxidation of NH_3 over it, thus the nitrogen-doped catalyst exhibited superior NO_x removal efficiency and N_2 selectivity [63]. Moreover, relevant studies had shown that the introduction of carbon could also change the magnetic and electron transfer characteristics of metal oxides and enhance the stability of metal oxides [57,64,65]. Therefore, the doping of non-metallic elements could exhibit a good improvement on the NH_3-SCR activity of cerium-based catalyst.

Melamine (1, 3, 5-triazine-2, 4, 6-triamine, $C_3H_6N_6$, Mel), a nitrogen-rich precursor with a high content of nitrogen element up to 66%, is predominately used in the production of fertilizers, flame retardants, photocatalysts or/and the nitrogen-doped materials via the thermal polymerization [66,67]. Interestingly, due to the similar structure and electronic characteristics of N and O atoms, the N-doped metallic oxide has also been deeply researched [68]. It was reported that the doping of N broadened the visible light response range of TiO_2, and the N-doped TiO_2 presented a good photocatalytic degradation performance for organic dyes and gaseous

acetaldehyde [69]. Wang et al. pointed out that the co-doping of C and N elements via a heat treatment of melamine significantly enhanced the photocatalytic activity of TiO_2 nanotube owing to their synergistic promotional effect [70]. Yao et al. found that the doping of N helped to enhance the electron donor effect and electron mobility of manganese-containing semi-coke catalyst, thus promoted its low-temperature NH_3-SCR activity [71]. However, there are few studies about the doping of nonmetallic elements (N or/and C) on the structure, chemical properties and NH_3-SCR activity of Ce-based catalyst via the co-pyrolysis of Mel.

In order to improve the NH_3-SCR activity of $Ce_{20}W_{10}Ti_{100}O_z$ catalyst and increase its practical application in reducing NO_x emission from the coal-fired power station, nonmetallic N or/and C are doped by the co-pyrolysis of Mel. The results indicated that the doping of N/C significantly improved the medium/low temperature NH_3-SCR activity of $Ce_{20}W_{10}Ti_{100}O_z$. Furthermore, the influence of N/C doping on the structure and physical properties of catalyst was thoroughly characterized by N_2 adsorption-desorption, X-ray diffraction (XRD), Raman spectra (Raman), X-ray photoelectron spectroscopy (XPS), Transmission electron microscope (TEM), Energy dispersive spectroscopy (TEM-EDS), NH_3 temperature-programmed desorption (NH_3-TPD) and Hydrogen temperature-programmed reduction (H_2-TPR).

2. Materials and methods

$Ce_{20}W_{10}Ti_{100}O_z$ were synthesized via the hydrothermal co-precipitation method with $Ce(NO_3)_3{\cdot}6H_2O$, $(NH_4)_6H_2W_{12}O_{40}{\cdot}nH_2O$ and $Ti(SO_4)_2$ as the precursors [72]. For the preparation of $Ce_{20}W_{10}Ti_{100}O_z$-Mel$_y$:Ti=x:2, $Ce(NO_3)_3{\cdot}6H_2O$, $(NH_4)_6H_2W_{12}O_{40}{\cdot}nH_2O$, $Ti(SO_4)_2$, excess urea and Mel were firstly dissolved in deionized water by keeping the molar ratio of Ce/W/Ti and the mass ratio of Mel/$Ti(SO_4)_2$ being 20:10:100 and x:2 (x=1,2,3,4), respectively. A pale-yellow

precipitate was obtained after being stirred vigorously at 90 °C for 12 h, and then the obtained precipitate was filtrated and washed by the de-ions water and the absolute ethanol. Finally, the dried precipitate was calcined at 550 °C for 5 h in a muffle furnace. The obtained catalyst was denoted as $Ce_{20}W_{10}Ti_{100}O_z$-Mel$_f$:Ti=x:2, where x represents the added dosage of Mel before the hydrothermal co-precipitation. Similar to the preparation of $Ce_{20}W_{10}Ti_{100}O_z$-Mel$_f$:Ti=x:2, $Ce_{20}W_{10}Ti_{100}O_z$-Mel$_t$:Ti=y:2(y=1,2,3,4) were synthesized by adding a certain of Mel into the mixed solution of the precipitate after the hydrothermal co-precipitation. Then, the mixed solution was hydrothermally treated at a certain temperature for 0 h, 2 h or 4 h, and the following process was the same as the preparation of $Ce_{20}W_{10}Ti_{100}O_z$-Mel$_f$:Ti=x:2. In comparison, $Ce_{20}W_{10}Ti_{100}O_z$-Mel$_f$:Mel$_t$:Ti=x:(4-x):2 (x=1,2) catalysts were also obtained by the distributed addition of Mel but the mass ratio of (Mel$_f$+Mel$_t$)/Ti$(SO_4)_2$ was kept at 4:2. The as-prepared $Ce_{20}W_{10}Ti_{100}O_z$-Mel$_t$:Ti=1:2 and $Ce_{20}W_{10}Ti_{100}O_z$-Mel$_t$:Ti=4:2 catalysts were characterized by a series of techniques to investigate the doping of C/N on the physical-chemical properties of $Ce_{20}W_{10}Ti_{100}O_z$, which were given in the supporting information.

The reaction conditions were controlled as follows: the used sample of 0.45 g, 600 ppm NO, 600 ppm NH_3, 5 vol.% O_2, N_2 balance, and 1500 mL/min total flow rate of the simulated flue gas, corresponding to a gas hourly space velocity (GHSV) of 200,000 mL/(g·h). The concentrations of NO_x at the inlet and outlet of the reactor were monitored online using a flue gas analyzer (testo350, Germany). NO conversion (X_{NOx}) was calculated by the equation as below:

$$X_{NOx}=(1-[NO_x]_{out}/[NO_x]_{in})\times 100\% \text{ with } [NO_x]=[NO]+[NO_2] \quad (1)$$

3. Results and discussions

3.1. Catalytic performance

Fig. 1(a) shows the influence of Mel modification before the hydrothermal co-precipitation on the NH_3-SCR activity of $Ce_{20}W_{10}Ti_{100}O_z$. It can be seen that $Ce_{20}W_{10}Ti_{100}O_z$-Mel$_f$:Ti=4:2 presents a little better catalytic performance than $Ce_{20}W_{10}Ti_{100}O_z$, especially the activity at 450～500 °C. This demonstrates that the addition of Mel before the hydrothermal co-precipitation doesn't substantially enhance the NH_3-SCR activity of $Ce_{20}W_{10}Ti_{100}O_z$. Therefore, we investigated the influence of Mel modification after the hydrothermal co-precipitation on the NH_3-SCR activity of $Ce_{20}W_{10}Ti_{100}O_z$ by keeping the mass ratio of Mel/$Ti(SO_4)_2$ also being 4:2. It was found that $Ce_{20}W_{10}Ti_{100}O_z$-Mel$_t$:Ti=4:2 exhibited higher catalytic performance at 150～450 °C than both $Ce_{20}W_{10}Ti_{100}O_z$ and $Ce_{20}W_{10}Ti_{100}O_z$-Mel$_f$:Ti=4:2, indicating that the addition of Mel after the hydrothermal co-precipitation presents a stronger promotional effect on the NH_3-SCR activity of catalyst. Interestingly, the qualities of these three dried samples after the hydrothermal co-precipitation decrease as follow: $Ce_{20}W_{10}Ti_{100}O_z$-Mel$_t$:Ti=4:2>$Ce_{20}W_{10}Ti_{100}O_z$-Mel$_f$:Ti=4:2 ≈$Ce_{20}W_{10}Ti_{100}O_z$. The main reason of this phenomenon is that the dry yellowish precipitate of $Ce_{20}W_{10}Ti_{100}O_z$-Mel$_t$:Ti=4:2 contains the white, salt-like crystalline particles which are the formed cyanuric acid from the slow hydrolysis of partial Mel. Meanwhile, the hydrolysis of Mel is related to the temperature and pH value of mixed solution [73]. Thus, the added Mel before the hydrothermal co-precipitation might be almost hydrolyzed when the mixed solution has been hydrothermally treated at 90 °C for 12 h [74], and the duration of hydrothermal treatment can affect the residual of Mel and cyanuric acid in the dried samples before the calcination. In addition, there still exists a large residual Mel and cyanuric acid in the dried precursor of $Ce_{20}W_{10}Ti_{100}O_z$-Mel$_t$:Ti=4:2 even if the added Mel solution has been hydrothermally treated at 90 °C for another 4 h, thus the duration of hydrothermal treatment lower than 4 h almost plays no

role on the promotional effect of Mel modification on the NH_3-SCR activity of $Ce_{20}W_{10}Ti_{100}O_z$. Interestingly, as shown in Fig.1(b) and (c), the hydrothermal temperature after adding Mel also presents a similar effect of the hydrothermal duration on the catalytic performance of the modified catalyst. Therefore, it can be deduced that the residual Mel or/and cyanuric acid in the dried samples might play an important influence on promoting the NH_3-SCR activity of $Ce_{20}W_{10}Ti_{100}O_z$ due to the generated reducing gas (NH_3) during the calcined pyrolysis of Mel or/and cyanuric acid. Sun et al. had proven that the treatment of NH_3 contributed to promoting the adsorbed oxygen formed on the surface of CeO_2 catalyst, thus improved its NH_3-SCR activity [75]. Furthermore, according to the results in Fig.1(d), the decrease of Mel/$Ti(SO_4)_2$ mass ratio from 4:2 to 1:2 slightly increases the NH_3-SCR activity of $Ce_{20}W_{10}Ti_{100}O_z$-Mel_t:Ti=4:2 at 150~250 ^oC, but the enhancement of Mel/$Ti(SO_4)_2$ mass ratio from 4:2 to 8:2 reduces its catalytic performance due to the formed carbon nitride(g-C_3N_4) from the calcined pyrolysis of large residual Mel or/and cyanuric acid [76]. Therefore, the $Ce_{20}W_{10}Ti_{100}O_z$-Mel_t:Ti=1:2 and $Ce_{20}W_{10}Ti_{100}O_z$-Mel_t:Ti=4:2 catalysts had been chosen to investigate the influence of C/N doping on the physical-chemical properties of $Ce_{20}W_{10}Ti_{100}O_z$ in the following sections.

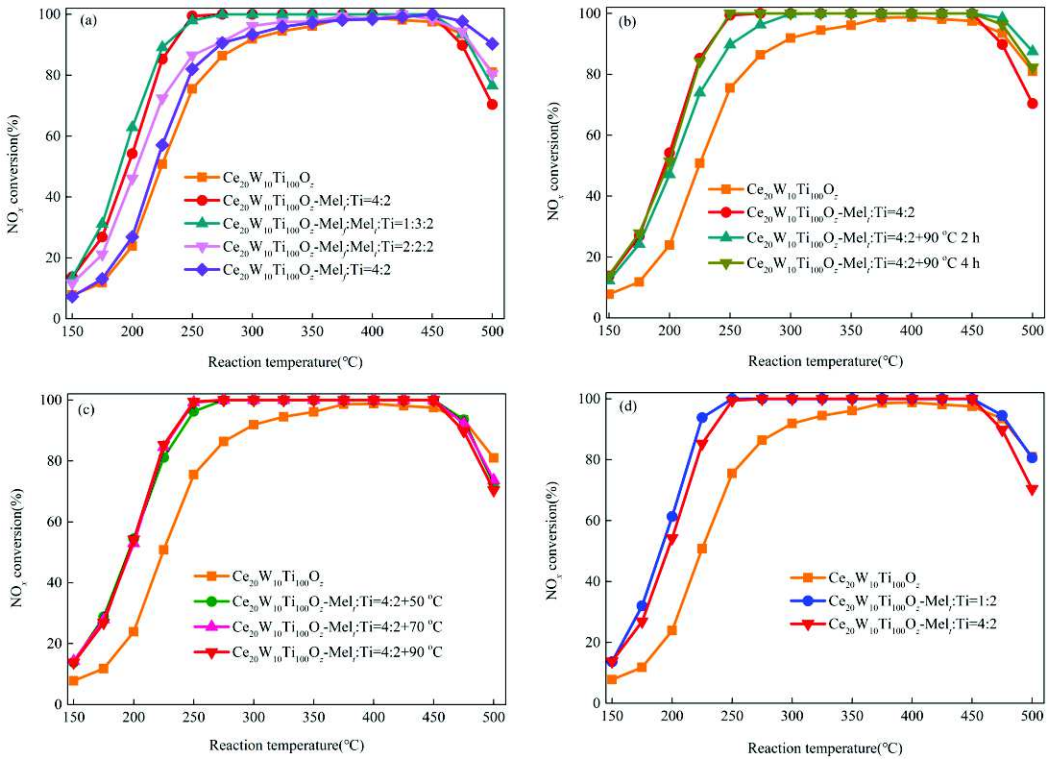

Fig.1. Influence of melamine modification on the NH_3-SCR activity of $Ce_{20}W_{10}Ti_{100}O_z$ catalyst ((a): The effect of addition amount of Mel; (b): The effect of hydrothermal duration after the introduction of Mel;(c): The hydrothermal temperature after the introduction of Mel; (d): The dosage of Mel. Reaction conditions: [NO]=[NH_3]=600 ppm, [O_2]=5 vol.%, balanced with N_2, 1500 mL/min total flow rate, 0.45 g of catalyst with GHSV of 200,000 mL/(g·h))

3.2. N_2 adsorption-desorption

Fig. 2(A) shows the N_2 adsorption-desorption isotherms of $Ce_{20}W_{10}Ti_{100}O_z$, $Ce_{20}W_{10}Ti_{100}O_z$-Mel$_t$:Ti=1:2 and $Ce_{20}W_{10}Ti_{100}O_z$-Mel$_t$:Ti=4:2. According to IUPAC classification, the isotherms of catalysts are attributed to type IV with the H_2 hysteresis loop, which indicates that they present meso-porous structure related to the capillary polycondensation in the mesopore range (2~50 nm) [77]. The BET surface area, pore volume and average pore diameter of catalysts are listed in Table 1. It can be seen that the enhancement of Mel/$Ti(SO_4)_2$ mass ratio from 1:2 to 4:2 strengthens the reducing effect of Mel modification on the BET surface area and pore volume

of $Ce_{20}W_{10}Ti_{100}O_z$. However, according to the results in Fig. 2(B), this modification refines the pore diameter of catalyst by making its pore size distribution shift to left, and contributes to the formation of the meso-porous of $Ce_{20}W_{10}Ti_{100}O_z$ at 2∼5 nm. In general, larger BET surface area helps to improve the adsorption of reactants on the surface of catalyst, thereby increases its NH_3-SCR activity [78]. Therefore, the modification of Mel after the hydrothermal co-precipitation decreases the BET surface area of $Ce_{20}W_{10}Ti_{100}O_z$, but increases its catalytic performance, and the BET surface area might not be the determining factor on affecting the NH_3-SCR activity of $Ce_{20}W_{10}Ti_{100}O_z$.

Table1 The micro-structure properties of $Ce_{20}W_{10}Ti_{100}O_z$, $Ce_{20}W_{10}Ti_{100}O_z$-Mel_t:Ti=1:2 and $Ce_{20}W_{10}Ti_{100}O_z$-Mel_t:Ti=4:2 catalysts

Samples	BET surface area [a] (m^2g^{-1})	Pore volume [b] (cm^3g^{-1})	Pore diameter [c] (nm)
$Ce_{20}W_{10}Ti_{100}O_z$	86.38	0.171	5.8
$Ce_{20}W_{10}Ti_{100}O_z$-Mel_t:Ti=1:2	84.66	0.141	4.8
$Ce_{20}W_{10}Ti_{100}O_z$-Mel_t:Ti=4:2	73.28	0.111	4.3

[a] BET surface area

[b] BJH desorption pore volume

[c] BJH desorption pore diameter

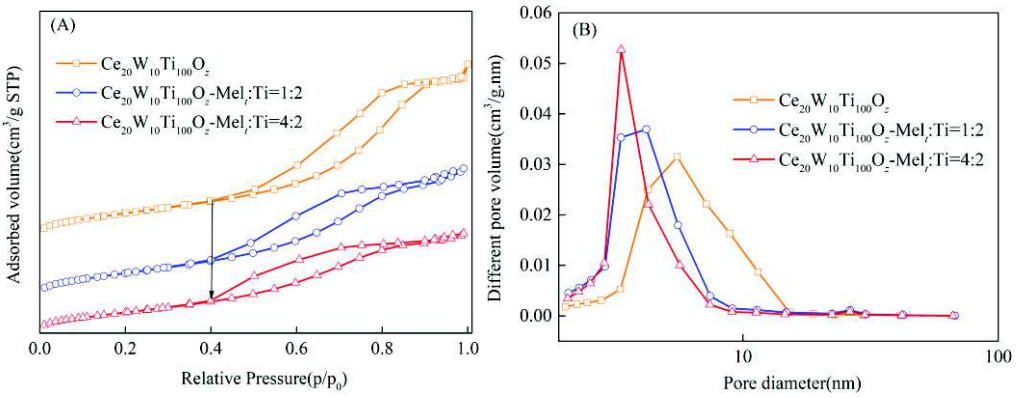

Fig.2. N_2 adsorption results of $Ce_{20}W_{10}Ti_{100}O_z$, $Ce_{20}W_{10}Ti_{100}O_z$-Mel$_t$:Ti=1:2 and $Ce_{20}W_{10}Ti_{100}O_z$-Mel$_t$:Ti=4:2 ((A) The N_2 adsorption-desorption isotherms, (B) The pore size distributions)

3.3 XRD and Raman

The XRD results of the as-prepared $Ce_{20}W_{10}Ti_{100}O_z$, $Ce_{20}W_{10}Ti_{100}O_z$-Mel$_t$:Ti=1:2 and $Ce_{20}W_{10}Ti_{100}O_z$-Mel$_t$:Ti=4:2 catalysts are illustrated in Fig. 3(A). It can be clearly seen that all catalysts exhibit the diffraction peaks of typical anatase TiO_2 (PDF#21-1272), but the modification of Mel decreases the intensity of diffraction peaks attributed to the anatase TiO_2 of $Ce_{20}W_{10}Ti_{100}O_z$. Furthermore, due to the calcined co-pyrolysis of the residual Mel and cyanuric acid, nonmetallic elements, including C or/and N, might be doped into the lattice of anatase TiO_2 crystallite, thus changes the crystal structure of catalyst [79]. The main reason is that the residual Mel and cyanuric acid in the dried precursor firstly thermally decomposes into the nitrogen-containing materials volatilized in the form of ammonia, and then aggregates into the carbon-nitrogen compounds, for example, Melem (2,5,8-triamino-tri-s- triazine) [80]. As a result, a certain of N or/and C elements might be doped into the lattice of anatase TiO_2 crystallite during the calcination, although the XRD diffractions of N/C nanocrystal had not been detected in the modified catalysts. It should be mentioned that the tungsten or cerium species present in amorphous or microcrystalline phase because no XRD diffraction peaks attributed to them were also detected

[56]. In general, the doped additives in an amorphous form contributes to enhancing the surface dispersion of active components, and easily lead to the lattice distortion of catalyst, thus significantly reduce the conductivity of oxides and promote the strong diffusion of ions, thereby resulting in the orderly arrangement of oxygen vacancies on the composite surface [81,82]. The results of Raman spectroscopy in Fig. 3(B) demonstrate that there exist four Raman peaks, located at around 154 cm^{-1}, 403 cm^{-1}, 522 cm^{-1} and 641 cm^{-1}, are attributed to the vibration mode of E_g, B_{1g}, A_{1g}/B_{2g} and E_g of anatase TiO_2, respectively [83], and no peaks are assigned to the species of cerium or tungsten obtained, confirming the existence of anatase TiO_2 and the high dispersion of active Ce or/and W species on the surface of catalysts. Furthermore, the modification of Mel slightly weakens the Raman spectroscopy intensity assigned to the anatase TiO_2 of $Ce_{20}W_{10}Ti_{100}O_z$ and inhibits its crystallite [49,84], which is in accordance with the results of XRD diffraction pattern.

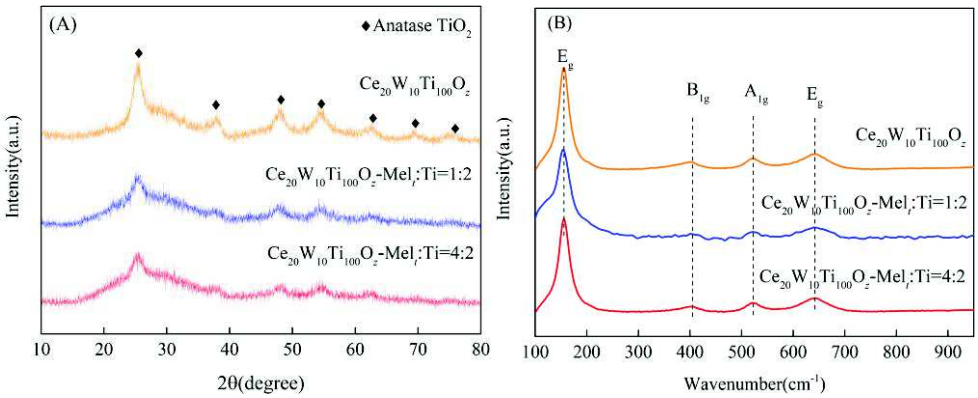

Fig.3. XRD patterns(A) and Raman spectroscopy(B) of $Ce_{20}W_{10}Ti_{100}O_z$, $Ce_{20}W_{10}Ti_{100}O_z$-Mel$_t$:Ti=1:2 and $Ce_{20}W_{10}Ti_{100}O_z$-Mel$_t$:Ti=4:2

3.4 XPS

XPS spectra was measured to investigate the influence of Mel modification on the chemical states of species and their concentrations on the surface of $Ce_{20}W_{10}Ti_{100}O_z$ with C1s (BE=284.6

256 eV) as the calibration. According to the full scan survey spectra of the catalysts depicted in Fig. S1.
257 It can be seen that that the XPS spectra of Ce 3d, W 4f, Ti 2p and O 1s have been detected, and
258 $Ce_{20}W_{10}Ti_{100}O_z$ exhibits the C 1s peak arising from the adventitious hydrocarbon exposure in the
259 instrument. However, the modification of Mel increases the intensity of the C 1s peak, and this
260 effect is further enhanced by increasing the Mel/$Ti(SO_4)_2$ mass ratio from 1:2 to 4:2, which
261 indicates that the modification of Mel contributes to doping carbon into the anatase TiO_2 of catalyst.
262 Furthermore, the Mel modification also induces the nitrogen element formed in
263 $Ce_{20}W_{10}Ti_{100}O_z$-Mel_t:Ti=1:2 and $Ce_{20}W_{10}Ti_{100}O_z$-Mel_t:Ti=4:2 according to the results in Fig.4(D).
264 Therefore, the modification of Mel helps to dope C or/and N species into the modified
265 $Ce_{20}W_{10}Ti_{100}O_z$ catalysts.

266 **Table 2.** XPS results of $Ce_{20}W_{10}Ti_{100}O_z$, $Ce_{20}W_{10}Ti_{100}O_z$-Mel_t:Ti=1:2 and $Ce_{20}W_{10}Ti_{100}O_z$-Mel_t:Ti=4:2 catalysts

Samples	Surface concentrations of elements and the calculated molar ratio (%)						
	Ce	W	Ti	O	N	$Ce^{3+}/(Ce^{3+}+Ce^{4+})$	$O_\alpha/(O_\alpha+O_\beta)$
$Ce_{20}W_{10}Ti_{100}O_z$	5.71	5.52	20.82	67.41	-	20.9	28.2
$Ce_{20}W_{10}Ti_{100}O_z$-Mel_t:Ti=1:2	5.22	5.29	21.30	67.63	0.57	25.2	33.5
$Ce_{20}W_{10}Ti_{100}O_z$-Mel_t:Ti=4:2	4.83	5.06	21.39	68.29	0.44	28.6	30.0

267 By fitting the Ce 3d XPS spectra into eight peaks as shown in Fig.4(A), it can be found that
268 both Ce^{3+}(u' and v') and Ce^{4+}(u, u", u"', v, v" and v"') species exist on the surface of
269 $Ce_{20}W_{10}Ti_{100}O_z$. Furthermore, the modification of Mel increases the calculated surface
270 $Ce^{3+}/(Ce^{3+}+Ce^{4+})$ molar ratio by promoting the conversion of Ce^{4+} to Ce^{3+} on the surface of
271 $Ce_{20}W_{10}Ti_{100}O_z$(20.9% as shown in Table 2), and this promotional effect can be further enhanced
272 by increasing the Mel/$Ti(SO_4)_2$ mass ratio from 1:2 to 4:2. Generally, the enrichment of Ce^{3+}

species has been considered to promote the generation of active oxygen on the surface of Ce-based catalyst and improves its catalytic oxidization of NO to NO_2, thus helps to promote the NH_3-SCR reaction [85]. Besides, the presence of Ce^{3+} species could lead to the imbalance of surface charge and the formation of unsaturated chemical bonds, thereby improving the chemisorption of oxygen on the surface of Ce-based catalyst. In general, a higher surface $Ce^{3+}/(Ce^{3+}+Ce^{4+})$ molar ratio contributes to enhance the redox performance of catalyst [63]. It is thus clear that the doping of C or/and N improves the redox performance of $Ce_{20}W_{10}Ti_{100}O_z$ by increasing its surface $Ce^{3+}/(Ce^{3+}+Ce^{4+})$ molar ratio via the modification of Mel. As shown in Fig. 4(B) and Table 2, both the lattice oxygen (529.8~530.1 eV, marked as O_β) and chemical adsorbed oxygen (531.00~532.50 eV, marked as O_α) present on the surface of the as-prepared catalysts [86], and the Mel modification indeed enhances the surface $O_\alpha/(O_\alpha+O_\beta)$ molar ratio of $Ce_{20}W_{10}Ti_{100}O_z$. It had been pointed out that the increase of surface oxygen defects contributed to increasing the Curie point and the conductivity of metal oxides, thereby affected the interaction of components in metal oxides [87,88]. Therefore, the presence of surface Ce^{3+} helps to create oxygen vacancies and increase the surface chemisorbed oxygen of catalyst, which is beneficial to the oxidation of NO to NO_2, thus improves the NH_3-SCR activity [46,89]. Meanwhile, $Ce_{20}W_{10}Ti_{100}O_z$-Mel_t:Ti=4:2 presents a lower surface $O_\alpha/(O_\alpha+O_\beta)$ molar ratio than $Ce_{20}W_{10}Ti_{100}O_z$-Mel_t:Ti=1:2, which isn't in accordance with the calculated surface $Ce^{3+}/(Ce^{3+}+Ce^{4+})$ molar ratios. This demonstrates that the surface chemical adsorbed oxygen not only comes from the redox couples of Ce^{3+}/Ce^{4+} formed on the surface of the as-prepared catalyst, but also might be affected by the difference of C or/and N doping owing to the influence of Mel dosage. As shown in Fig.S2, the W 4f XPS spectra of samples can be fitted into two peaks, attributing to W $4f_{7/2}$(35.6 eV) and W $4f_{5/2}$(37.5 eV), respectively. Thus,

295 tungsten exists in W^{6+} species on the surface of catalysts [49,84]. Meanwhile, the Mel
296 modification lowers the W4f electron binding energy of $Ce_{20}W_{10}Ti_{100}O_z$ by increasing the electron
297 cloud density of surface tungsten species, thus changes the chemical environment around them.
298 Furthermore, the doping of C or/and N into the lattice of anatase TiO_2 via Mel modification also
299 lowers the binding energy of Ti 2p on the surface of $Ce_{20}W_{10}Ti_{100}O_z$ by decreasing the electron
300 cloud density around Ti^{4+} ion [90,91]. This is in accordance with the previous studies about the
301 reducing effect of nitrogen doping on the binding energy of Ti 2p [92,93].

302 The results of N 1s spectra in Fig.4(D) also confirms the doping of N into the Mel-modified
303 catalysts with one N1 s peak centered at 398.7 eV observed over $Ce_{20}W_{10}Ti_{100}O_z$-Mel_t:Ti=1:2 and
304 $Ce_{20}W_{10}Ti_{100}O_z$-Mel_t:Ti=4:2, and this peak might be attributed to the doped nitrogen element by
305 replacing the lattice oxygen of TiO_2 crystallite via the N-Ti-N bond [94]. After the modification of
306 Mel, $Ce_{20}W_{10}Ti_{100}O_z$-Mel_t:Ti=1:2 and $Ce_{20}W_{10}Ti_{100}O_z$-Mel_t:Ti=4:2 presents stronger C 1s
307 spectrum than $Ce_{20}W_{10}Ti_{100}O_z$. This demonstrates that carbon element has also been doped into
308 the above catalyst via the Mel modification. At the same time, the C 1s spectrum of the modified
309 catalysts can be deconvoluted into three main peaks located at 284.4 eV, 286.3 eV and 288.7 eV,
310 which correspond to the adventitious carbon impurities, C=N groups, and sp^2-bonded carbon of
311 the N-C=N coordination, respectively [95,96]. Furthermore, $Ce_{20}W_{10}Ti_{100}O_z$-Mel_t:Ti=4:2 exhibits
312 larger carbon surface concentration than $Ce_{20}W_{10}Ti_{100}O_z$-Mel_t:Ti=1:2. Because the XPS spectra
313 were calibrated by C 1s (BE=284.6 eV), the surface concentrations of Ce, W, Ti, O and N
314 elements were calculated according to the XPS results without considering the doped carbon
315 content. As shown in Table 2, the Mel modification effectively enlarges the surface concentrations
316 of Ti/O species and increases the dispersion of Ce/W species on the surface of $Ce_{20}W_{10}Ti_{100}O_z$.

This also leads to the doping of C or/and N elements into the modified catalyst and improves its surface $Ce^{3+}/(Ce^{3+}+Ce^{4+})$ molar ratio, thereby enhances the chemical adsorbed oxygen (O_α) concentration and $O_\alpha/(O_\alpha+O_\beta)$ molar ratio on the surface of $Ce_{20}W_{10}Ti_{100}O_z$. However, the increase of Mel/$Ti(SO_4)_2$ mass ratio from 1:2 to 4:2 decreases the doping content of N species with more carbon formed in the catalyst. This reduces the chemical adsorbed oxygen (O_α) concentration and $O_\alpha/(O_\alpha+O_\beta)$ molar ratio on the surface of the Mel modified catalyst. In addition, the surface O_α is generally considered as one important factor on the catalytic performance of NO_x reduction, and the NH_3-SCR activity of the catalysts decreases as follows: $Ce_{20}W_{10}Ti_{100}O_z$-Mel$_t$:Ti=1:2> $Ce_{20}W_{10}Ti_{100}O_z$-Mel$_t$:Ti=4:2>$Ce_{20}W_{10}Ti_{100}O_z$, which indicates that the chemical adsorbed oxygen (O_α) might play an important role on the NH_3-SCR activity of the Mel modified $Ce_{20}W_{10}Ti_{100}O_z$ catalyst.

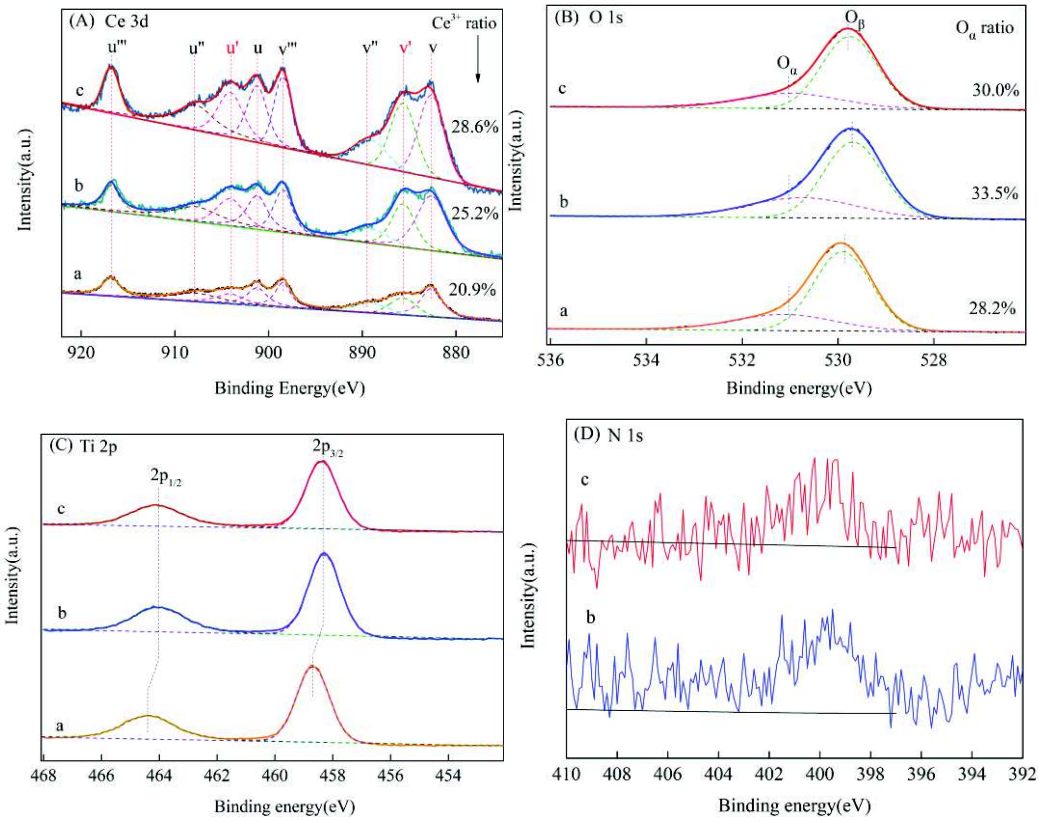

Fig.4. The XPS spectra of (a) $Ce_{20}W_{10}Ti_{100}O_z$, (b) $Ce_{20}W_{10}Ti_{100}O_z$-Mel$_t$:Ti=1:2 and (c) $Ce_{20}W_{10}Ti_{100}O_z$-Mel$_t$:Ti=4:2

catalysts ((A) Ce 3d, (B) O 1s, (C) Ti 2p, (D) N 1s)

3.5 HR-TEM and EDS

In order to investigate the influence of Mel modification on the microstructure of catalyst, especially the surface dispersion characteristics of the doped C or/and N, $Ce_{20}W_{10}Ti_{100}O_z$ and $Ce_{20}W_{10}Ti_{100}O_z$-Mel_t:Ti=4:2 had been chosen to be characterized by HR-TEM/EDS, and the results are given in Fig. 5 and 6. As shown in Fig.5, $Ce_{20}W_{10}Ti_{100}O_z$-Mel_t:Ti=4:2 presents graver particle agglomeration than $Ce_{20}W_{10}Ti_{100}O_z$ due to the doping of C or/and N. This result is consistent with the effect of Mel modification on reducing the specific surface area/pore volume of $Ce_{20}W_{10}Ti_{100}O_z$ and the XRD diffraction of anatase TiO_2 crystallite. According to the HR-TEM image in Fig. 5(b) and (d), the lattice fringe (d) of 0.352 nm ascribed to the crystal plane of anatase TiO_2 (101) is observed on the surface of both $Ce_{20}W_{10}Ti_{100}O_z$ and $Ce_{20}W_{10}Ti_{100}O_z$-Mel_t:Ti=4:2 [50], which demonstrates that the doping of C or/and N can't regulate the exposed crystal plane of anatase TiO_2 on the catalyst surface. Moreover, no lattice fringes attributed to the cerium or tungsten species are observed and they present in amorphous or highly dispersive microcrystalline phase, which are in accordance with the results of XRD and Raman. From the HR-TEM-EDS mappings results in Fig.6, it can be clearly seen that $Ce_{20}W_{10}Ti_{100}O_z$ exhibits high dispersion of Ce, W, Ti and O elements on its surface. Meanwhile, the Mel modification not only leads to the agglomerate distribution of these main components, but also promotes the formation of C and N elements on the surface of catalyst. This result confirms that C and N have been doped into $Ce_{20}W_{10}Ti_{100}O_z$ catalyst via the Mel modification, which improves the catalytic performance of $Ce_{20}W_{10}Ti_{100}O_z$.

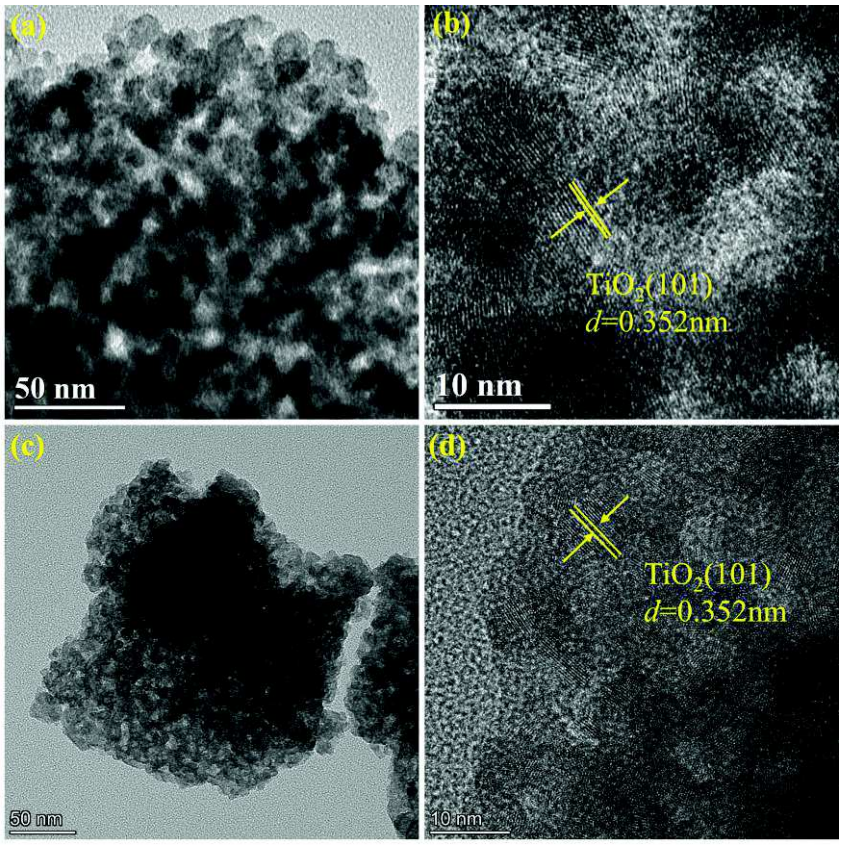

352

353 Fig.5. HR-TEM and TEM images of $Ce_{20}W_{10}Ti_{100}O_z$ (a-b) and $Ce_{20}W_{10}Ti_{100}O_z$-Mel_t:Ti=4:2 (c-d) catalysts

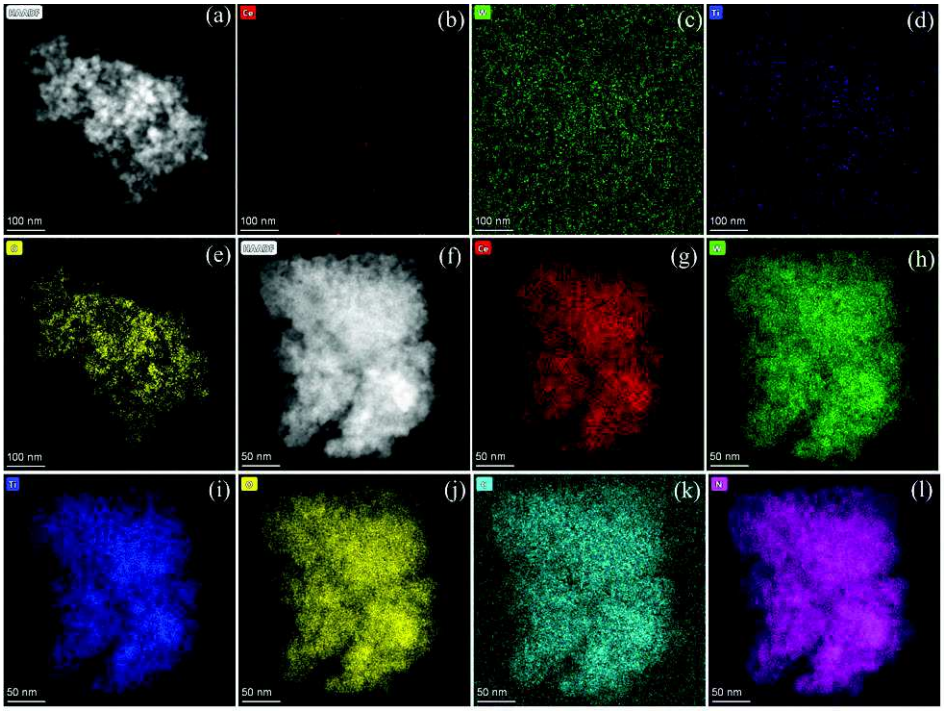

354

355 Fig.6. TEM-EDS mapping of $Ce_{20}W_{10}Ti_{100}O_z$ (a-e) and $Ce_{20}W_{10}Ti_{100}O_z$-Mel_t:Ti=4:2 (f-l) catalysts

356 **3.6 H_2-TPR**

The redox ability plays a significant impact on the catalytic performance of NO_x reduction due to the promotional activation of ammonia and NO_x on the surface of catalyst [97]. Thus, the H_2-TPR technology had been used to study the influence of Mel modification on the redox properties of $Ce_{20}W_{10}Ti_{100}O_z$ herein. As shown in Fig. 7, the H_2-TPR spectra of $Ce_{20}W_{10}Ti_{100}O_z$ can be de-convoluted into several sub-peaks at the temperature range of 400~650 °C. Among them, the peaks centered at 470 °C and 560 °C are attributed to the reduction of the surface or sub-surface oxygen, which come from the stoichiometric ceria of type Ce^{4+}-O-Ce^{4+} and the nonstoichiometric ceria of type Ce^{3+}-O-Ce^{4+} [98]. And, the reduction peaks at 501~536 °C are also assigned to the reduction of surface/subsurface oxygen from ceria [99] Moreover, it had been pointed out that the reduction peaks at around 501 °C and 437 °C could be ascribed to the reduction of surface Ce^{4+} to Ce^{3+} and WO_3 to $WO_{2.9}$, respectively [46,100]. Thus, the modification of Mel increases the reduction temperature of the surface or sub-surface oxygen, the surface Ce^{4+} to Ce^{3+} and WO_3 to $WO_{2.9}$ for $Ce_{20}W_{10}Ti_{100}O_z$, and makes its H_2-TPR spectra shift to high temperatures. However, $Ce_{20}W_{10}Ti_{100}O_z$-Mel_t:Ti=1:2 presents stronger H_2-TPR spectra than $Ce_{20}W_{10}Ti_{100}O_z$, which shows that the Mel modification optimizes the reducibility of the surface oxygen and active Ce/W species of catalyst when the Mel/$Ti(SO_4)_2$ mass ratio is 1:2, especially the surface or sub-surface oxygen. Interestingly, $Ce_{20}W_{10}Ti_{100}O_z$-Mel_t:Ti=4:2 presents higher surface/sub-surface oxygen relative concentrations (Molar ratio) than $Ce_{20}W_{10}Ti_{100}O_z$-Mel_t:Ti=1:2. Therefore, the Mel modification enlarges the reduction temperature owing to more Ti species formed on the surface of $Ce_{20}W_{10}Ti_{100}O_z$, but increases its surface/sub-surface oxygen relative concentrations due to the doping of C or/and N. Meanwhile, the dosage of Mel can regulate the amount of Ti species, doped C or/and N elements on the

surface of catalyst, thus affects its reducibility. In general, the redox properties are positively correlated with the activity of catalyst [101]. In this study, $Ce_{20}W_{10}Ti_{100}O_z$-Mel$_t$:Ti=1:2 and $Ce_{20}W_{10}Ti_{100}O_z$-Mel$_t$:Ti=4:2 present better NO_x conversion at the test reaction temperature, while they exhibit higher surface/sub-surface oxygen relative concentrations, which are in accordance with the XPS results.

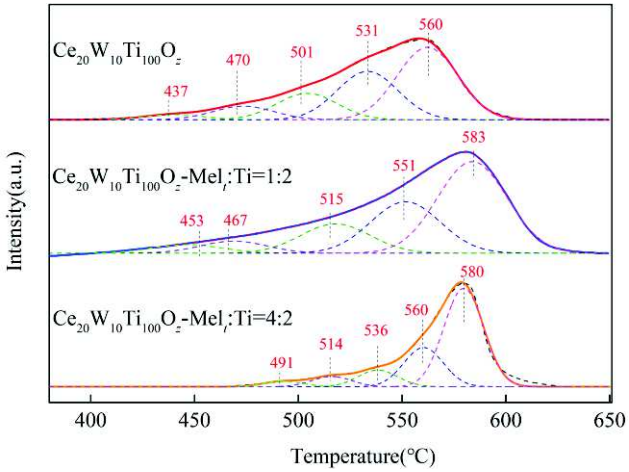

Fig.7. H_2-TPR curves of $Ce_{20}W_{10}Ti_{100}O_z$, $Ce_{20}W_{10}Ti_{100}O_z$-Mel$_t$:Ti=1:2 and $Ce_{20}W_{10}Ti_{100}O_z$-Mel$_t$:Ti=4:2 catalysts

3.7 NH_3-TPD

It has been established that the surface acidity plays a significant role on the NH_3-SCR reaction of catalyst [102]. In our previous study, it had been pointed out that two NH_3 desorption peaks were obtained for $Ce_{20}W_{10}Ti_{100}O_z$. Among them, the low-temperature peak is attributed to the physically adsorbed NH_3 and the partial ionic NH_4^+ bound to the weak Brønsted acid sites. And the middle-temperature peak is imputed to the coordinated NH_3 bound to the Lewis acid sites and the ionic NH_4^+ bound to the strong Brønsted acid sites [56]. Herein, in order to confirm the thermal stability of adsorbed NH_3 species bound to the Lewis acid sites or/and strong Brønsted acid sites and prevent the desorption of the doped C or/and N groups under the temperature higher than 400 °C, a new test method had been adopted to measure the NH_3-TPD of $Ce_{20}W_{10}Ti_{100}O_z$-Mel$_t$:Ti=1:2 and

$Ce_{20}W_{10}Ti_{100}O_z$-Mel_t:Ti=4:2 by introducing a two-hour durative desorption of ammonia species at 350 °C. By comparing our previous research [56] and the results in Fig. 8, it can be found that the Mel modification decreases the low-temperature NH_3 desorption properties of $Ce_{20}W_{10}Ti_{100}O_z$, but $Ce_{20}W_{10}Ti_{100}O_z$-Mel_t:Ti=1:2 presents stronger surface acidity than $Ce_{20}W_{10}Ti_{100}O_z$-Mel_t:Ti=4:2 at the tested temperature range. Interestingly, after a two-hour durative desorption of NH_3 species at 350 °C, the two modified catalysts exhibit similar desorption properties of NH_3 species when the desorbed temperature increases from 350 to 500 °C. This demonstrates that the adsorbed NH_3 species can be almost completely desorbed at the temperature lower than 350 °C and the enhancement of Mel/$Ti(SO_4)_2$ mass ratio decreases the surface acid sites of $Ce_{20}W_{10}Ti_{100}O_z$-Mel_t:Ti=1:2, which is in accordance with its effect on the NH_3-SCR activity.

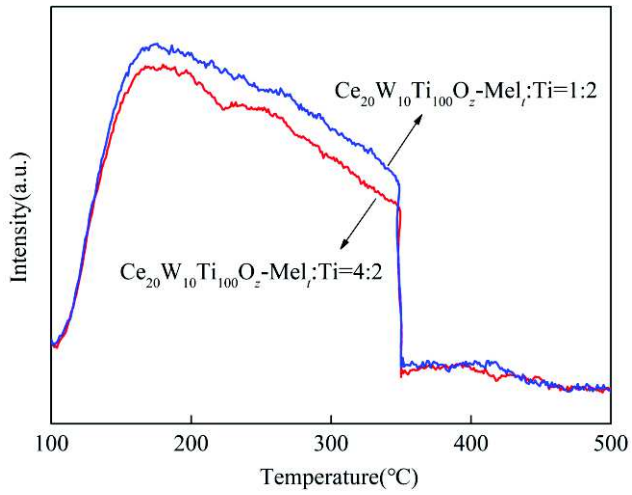

Fig.8. NH_3-TPD curves of $Ce_{20}W_{10}Ti_{100}O_z$-Mel_t:Ti=1:2 and $Ce_{20}W_{10}Ti_{100}O_z$-Mel_t:Ti=4:2 catalysts

4. Conclusions

In this paper, melamine (Mel), the nitrogen and carbon-rich material, was firstly used to promote the NH_3-SCR activity of $Ce_{20}W_{10}Ti_{100}O_z$ catalyst via the doping of nonmetallic elements. The characterization results demonstrate that the Mel modification after the hydrothermal co-precipitation helps to dope C or/and N into the lattice of anatase TiO_2 crystallite for

413 $Ce_{20}W_{10}Ti_{100}O_z$ and thus reduces the intensity of the XRD diffraction and Raman spectroscopy
414 attributed to anatase TiO_2. In addition, the Mel modification enhances the dispersion of tungsten
415 and cerium species, which present in amorphous or microcrystalline phase on the surface of
416 $Ce_{20}W_{10}Ti_{100}O_z$. In addition, the doping of C or/and N elements after the Mel modification
417 increases the surface $Ce^{3+}/(Ce^{3+}+Ce^{4+})$ molar ratio of catalyst by promoting the conversion of
418 partial Ce^{4+} to Ce^{3+}, thus increases its surface concentration of chemical adsorbed oxygen(O_α). The
419 high dispersion of metal elements, more surface Ce^{3+} and larger chemisorbed oxygen ratio
420 contribute to promoting the oxidation of NO to NO_2, which is conducive to the "fast SCR"
421 reaction. Meanwhile, $Ce_{20}W_{10}Ti_{100}O_z$-Mel_t:Ti=1:2 presents stronger surface acidity and larger
422 surface $O_\alpha/(O_\alpha+O_\beta)$ molar ratio than $Ce_{20}W_{10}Ti_{100}O_z$-Mel_t:Ti=4:2, which might be the important
423 reasons for its better catalytic performance. Finally, the influence of Mel adding method, Mel
424 dosage, hydrothermal temperature and duration time on the NH_3-SCR activity of the modified
425 $Ce_{20}W_{10}Ti_{100}O_z$ catalyst had also been investigated. $Ce_{20}W_{10}Ti_{100}O_z$-Mel_t:Ti=1:2 achieves higher
426 than 98% NO_x conversion at an abroad window temperature range of 250～450 °C and presents the
427 best catalytic performance. The research results provide an effective strategy for optimizing the
428 NH_3-SCR activity of CeWTi catalyst and are valuable to develop the high-efficiency and low-cost
429 modified composite metal-based catalyst for NO_x reduction.

430 **Acknowledgements**

431 This work was supported by the National Science Foundation of China (No. 51406118),
432 Program of Special Appointment (Eastern Scholar) at Shanghai Institutions of Higher Learning
433 (No. QD2015017). The Bureau of Huzhou Municipal Science and Technology (NO.
434 2021ZD2043).

Availability of data and materials

All data generated or analyzed during this study are included in this published article and its supplementary information files.

References

[1] X. Wu, L.L. Liu, J.N. Liu, B.H. Hou, Y.L. Du, X.M. Xie, NiMn mixed oxides with enhanced low-temperature deNO$_x$ performance: Insight into the coordinated decoration of MnO$_x$ by NiO phase via glycine combustion method, Appl. Catal. A Gen. 610 (2021) 117918, https://doi.org/10.1016/j.apcata.2020.117918.

[2] Z.H. Wang, M.Y. Jiao, Z.P. Chen, H. He, L.C. Liu, Effects of montmorillonite and anatase TiO$_2$ support on CeO$_2$ catalysts during NH$_3$-SCR reaction, Micropor. Mesopor. Mat. 320 (2021) 111072, https://doi.org/10.1016/j.micromeso.2021.111072.

[3] M.Y. Guo, Q.L. Liu, C.X. Liu, X.H. Wang, Y.L. Bi, B.Y. Fan, D.G. Ma, X.Y. Liang, Z.G. Li, Rational design of novel CrZrO$_x$ catalysts for efficient low temperature SCR of NO$_x$, Chem. Eng. J. 413 (2021) 127554, https://doi.org/10.1016/j.cej.2020.127554.

[4] J.Y. Chen, B.Z. Zhu, W.Y. Song, Y.L. Sun, Catalytic performance of calcined Fe$_2$O$_3$/CA catalyst for NH$_3$-SCR reaction: Role of activation temperature, J. Solid State Chem. 316 (2022) 123630, https://doi.org/10.1016/j.jssc.2022.123630.

[5] J. Arfaoui, A. Ghorbel, C. Petitto, G. Delahay, Promotional effect of ceria on the catalytic behaviour of new V$_2$O$_5$-WO$_3$-TiO$_2$ aerogel solids for the deNO$_x$ process, J. Solid State Chem. 300 (2021) 122261, https://doi.org/10.1016/j.jssc.2021.122261.

[6] H.L. Wu, M.Y. He, W.Z. Liu, L.J. Jiang, J. Cao, C. Yang, J. Yang, J. Peng, Y. Liu, Q.C. Liu, Application of manganese-containing soil as novel catalyst for low-temperature NH$_3$-SCR of NO, J. Environ. Chem. Eng. 9 (2021) 105426, https://doi.org/10.1016/j.jece.2021.105426.

[7] X. Wu, R.N. Wang, Y.L. Du, C.L. Zou, H. Meng, X.M. Xie, Performance enhancement of NH_3-SCR via employing hydrotalcite-like precursor to induce the decoration of NiO by TiO_2 phase, Mol. Catal. 467 (2019) 150–160, https://doi.org/10.1016/j.mcat.2019.02.004.

[8] C.X. Li, Z.B. Xiong, J.F. He, X.K. Qu, Z.Z. Li, X. Ning, W. Lu, S.M. Wu, L.Z. Tan, Influence of ignition atmosphere on the structural properties of magnetic iron oxides synthesized via solution combustion and the NH_3-SCR activity of W/Fe_2O_3 catalyst, Appl. Catal. A Gen. 602 (2020) 117726, https://doi.org/10.1016/j.apcata.2020.117726.

[9] K.B. Nam, S.H. Lee, S.C. Hong, The role of copper in the enhanced performance of W/Ti catalysts for low-temperature selective catalytic reduction, Appl Surf Sci. 544 (2021) 148643, https://doi.org/10.1016/j.apsusc.2020.148643.

[10] S.R. Yousefi, M. Ghanbari, O. Amiri, Z. Marzhoseyni, P. Mehdizadeh, M. Hajizadeh-Oghaz, M. Salavati-Niasari, $Dy_2BaCuO_5/Ba_4DyCu_3O_{9.09}$ S-scheme heterojunction nanocomposite with enhanced photocatalytic and antibacterial activities, J. Am. Ceram. Soc. 104 (2021) 2952–2965, https://doi.org/10.1111/jace.17696.

[11] S. Sangeetha, G. Krishnamurthy, Electrochemical and photocatalytic applications of Ce-MOF, Bull Mater Sci. 43 (2020) 269. https://doi.org/10.1016/j.apsusc.2020.148643.

[12] S.R. Yousefi, O. Amiri, M. Salavati-Niasari, Control sonochemical parameter to prepare pure $Zn_{0.35}Fe_{2.65}O_4$ nanostructures and study their photocatalytic activity, Ultrason. Sonochem. 58 (2019) 104619, https://doi.org/10.1016/j.ultsonch.2019.104619.

[13] S.R. Yousefi, H.A. Alshamsi, O. Amiri, M. Salavati-Niasari, Synthesis, characterization and application of Co/Co_3O_4 nanocomposites as an effective photocatalyst for discoloration of organic dye contaminants in wastewater and antibacterial properties, J. Mol. Liq. 337 (2021) 116405,

https://doi.org/10.1016/j.molliq.2021.116405.

[14] S.R. Yousefi, M. Masjedi-Arani, M.S. Morassaei, M. Salavati-Niasari, H. Moayedi, Hydrothermal synthesis of $DyMn_2O_5/Ba_3Mn_2O_8$ nanocomposite as a potential hydrogen storage material, Int. J. Hydrogen Energ. 44 (2019) 24005–24016, https://doi.org/10.1016/j.ijhydene.2019.07.113.

[15] S.R. Yousefi, A. Sobhani, H.A. Alshamsic, M. Salavati-Niasari, Green sonochemical synthesis of $BaDy_2NiO_5/Dy_2O_3$ and $BaDy_2NiO_5$/NiO nanocomposites in the presence of core almond as a capping agent and their application as photocatalysts for the removal of organic dyes in water, RSC Adv. 11 (2021) 11500–11512, https://doi.org/10.1039/D0RA10288A.

[16] J. Wang, H.C. Xuan, L.X. Meng, X.H. Liang, Y.P. Li, J. Yang, P.D. Han, N, S co-doped $NiCo_2O_4$@$CoMoO_4$/NF hierarchical heterostructure as an efficient bifunctional electrocatalyst for overall water splitting, Int. J. Hydrogen Energ. In Press, https://doi.org/10.1016/j.ijhydene.2022.11.253.

[17] S. Manzoor, S.V. Trukhanov, M.N. Ansari, M. Abdullah, A. Alruwaili, A.V. Trukhanov, M.U. Khandaker, A.M. Idris, K.S. EI-Nasser, T.A. Taha, Flowery In_2MnSe_4 novel electrocatalyst developed via anion exchange strategy for efficient water splitting, Nanomaterials. 12 (2022) 2209. https://doi.org/10.3390/nano12132209.

[18] M. Hassan, Y. Slimani, M.A. Gondal, M.J.S. Mohamed, S. Güner, M.A. Almessiere, A.M. Surrati, A. Baykal, S. Trukhanov, A. Trukhanov, Structural parameters, energy states and magnetic properties of the novel Se-doped $NiFe_2O_4$ ferrites as highly efficient electrocatalysts for HER, Ceram. Int. 48 (2022) 24866-24876. https://doi.org/10.1016/j.ceramint.2022.05.140.

[19] X.J. Yao, L. Chen, J. Cao, Y. Chen, M. Tian, F.M. Yang, J.F. Sun, C.J. Tang, L. Dong, Enhancing the deNO_x performance of MnO_x/CeO_2-ZrO_2 nanorod catalyst for low-temperature NH_3-SCR by TiO_2 modification, Chem. Eng. J. 369 (2019) 46–56, https://doi.org/10.1016/j.cej.2019.03.052.

[20] F.Y. Gao, C. Yang, X.L. Tang, H.H. Yi, C.Z. Wang, One-step synthesis by redox co-precipitation method for

low-dimensional Me-Mn bi-metal oxides (Me=Co, Ni, Sn) as SCR DeNO$_x$ catalysts, Environ. Sci Pollut Res. 29 (2022) 21210–21220, https://doi.org/10.1007/s11356-021-14644-5.

[21] G.N. Özyönüm, R. Yildirim, Water gas shift activity of Au–Re catalyst over microstructured cordierite monolith wash-coated by ceria, Int. J. Hydrogen Energ. 41 (2016) 5513–5521, https://doi.org/10.1016/j.ijhydene.2016.02.025.

[22] D.H. Lee, T. Kim, Effect of Catalyst Deactivation on Kinetics of Plasma-Catalysis for Methanol Decomposition, Plasma. Process. Polym. 11 (2014) 455–463, https://doi.org/10.1002/ppap.201300185.

[23] V.A. Turchenko, A.V. Trukhanov, I.A. Bobrikov, S.V. Trukhanov, A.M. Balagurov, Investigation of the crystal and magnetic structures of $BaFe_{12-x}Al_xO_{19}$ solid solutions (x = 0.1-1.2), Crystallogr. Rep. 60 (2015) 629–635, https://doi.org/10.1134/S1063774515030220.

[24] M.V. Zdorovets, A.L. Kozlovskiy, D.I. Shlimas, D.B. Borgekov, Phase transformations in FeCo-Fe_2CoO_4/Co_3O_4-spinel nanostructures as a result of thermal annealing and their practical application, J. Mater. Sci.: Mater. Electron. 32 (2021) 16694–16705, https://doi.org/10.1007/s10854-021-06226-5.

[25] D.A. Vinnik, A.Yu. Starikov, V.E. Zhivulin, K.A. Astapovich, V.A. Turchenko, T.I. Zubar, S.V. Trukhanov, J. Kohout, T. Kmječ, O. Yakovenko, L. Matzui, A.S.B. Sombra, D. Zhou, R.B. Jotania, C. Singh, Y. Yang, A.V. Trukhanov, Changes in structure, magnetizatin and resistivity of $BaFe_{12-x}Ti_xO_{19}$, ACS Appl. Electron. Mater, 3 (2021) 1583–1593. https://dx.doi.org/10.1021/acsaelm.0c01081.

[26] K. Tanwar, D.S. Gyan, P. Gupta, S. Pandey, OmParkash, D. Kumar, Investigation of crystal structure, microstructure and low temperature magnetic behavior of Ce^{4+} and Zn^{2+} co-doped barium hexaferrites ($BaFe_{12}O_{19}$), RSC Adv. 8 (2018) 19600–19609, https://doi.org/10.1039/C8RA02455C.

[27] A. Anantharaman, S.G. Hashwene Priya, P.A. Vinosha, M. George, Structural, optical and photocatalytic activity of cerium titanium ferrite, Optik. 143 (2017) 71–83, https://doi.org/10.1016/j.ijleo.2017.06.059.

[28] H.D. Xu, X. Feng, S. Liu, Y. Wang, M.M. Sun, J.L. Wang, Y.Q. Chen, Promotional effects of Titanium additive on the surface properties, active sites and catalytic activity of W/$CeZrO_x$ monolithic catalyst for the selective catalytic reduction of NO_x with NH_3, Appl Surf Sci. 419 (2017) 697 – 707, https://doi.org/10.1016/j.apsusc.2017.05.055.

[29] X.J. Yao, L. Chen, J. Cao, Y. Chen, M. Tian, F.M. Yang, J.F. Sun, C.J. Tang, L. Dong, Enhancing the deNO_x performance of MnO_x/CeO_2-ZrO_2 nanorod catalyst for low-temperature NH_3-SCR by TiO_2 modification, Chem. Eng. J. 369 (2019) 46–56, https://doi.org/10.1016/j.cej.2019.03.052.

[30] F.Y. Gao, Y.Y. Liu, Z. Sani, X.L. Tang, H.H. Yi, S.Z. Zhao, Q.J. Yu, Y.S. Zhou, Advances in selective catalytic oxidation of ammonia (NH_3-SCO) to dinitrogen in excess oxygen: A review on typical catalysts, catalytic performances and reaction mechanisms, J. Environ. Chem Eng. 9 (2021) 104575, https://doi.org/10.1016/j.jece.2020.104575.

[31] Y.H. Zhou, S. Ren, J. Yang, W.Z. Liu, Z.H. Su, Z.C. Chen, M.M. Wang, L. Chen, Effect of oxygen vacancies on improving NO oxidation over CeO_2 {111} and {100} facets for fast SCR reaction, J. Environ. Chem Eng. 9 (2021) 106218, https://doi.org/10.1016/j.jece.2021.106218.

[32] D.I. Shlimas, A.L. Kozlovskiy, M.V. Zdorovets, Study of the formation effect of the cubic phase of $LiTiO_2$ on the structural, optical, and mechanical properties of Li2±xTi1±xO3 ceramics with different contents of the X component, J. Mater. Sci.: Mater. Electron. 32 (2021) 7410 – 7422. https://doi.org/10.1007/s10854-021-05454-z.

[33] N.A. Algarou, Y. Slimani, M.A. Almessiere, F.S. Alahmari, M.G. Vakhitov, D.S. Klygach, S.V. Trukhanov, A.V. Trukhanov, A. Baykal, Magnetic and microwave properties of $SrFe_{12}O_{19}$/$MCe_{0.04}Fe_{1.96}O_4$ (M = Cu, Ni, Mn, Co and Zn) hard/soft nanocomposites, J. Mater. Res. Technol. 9 (2020) 5858 – 5870, https://doi.org/10.1016/j.jmrt.2020.03.113.

[34] A.L. Kozlovskiy, M.V. Zdorovets, Effect of doping of $Ce^{4+/3+}$ on optical, strength and shielding properties of (0.5-x)TeO_2-0.25MoO-0.25Bi_2O_3-xCeO_2 glasses, Mater. Chem. Phys. 263 (2021) 124444 , https://doi.org/10.1016/j.matchemphys.2021.124444.

[35] Z.B. Xiong, Z.Z. Li, C.X. Li, W. Wang, W. Lu, Y.P. Du, S.L. Tian, Green synthesis of Tungsten-doped CeO_2 catalyst for selective catalytic reduction of NO_x with NH_3 using starch bio-template, Appl Surf Sci. 536 (2021) 147719, https://doi.org/10.1016/j.apsusc.2020.147719.

[36] J. Yang, S. Ren, T.S. Zhang, Z.H. Su, H.M. Long, M. Kong, L. Yao, Iron doped effects on active sites formation over activated carbon supported Mn-Ce oxide catalysts for low-temperature SCR of NO, Chem. Eng. J. 379 (2020) 122398, https://doi.org/10.1016/j.cej.2019.122398.

[37] K. Zhao, W.L. Han, G.X. Lu, J.Y. Lu, Z.C. Tang, X.P. Zhen, Promotion of redox and stability features of doped Ce-W-Ti for NH_3-SCR reaction over a wide temperature range, Appl Surf Sci. 379 (2016) 316–322, https://doi.org/10.1016/j.apsusc.2016.04.090.

[38] F.Y. Gao, X.L. Tang, H.H. Yi, J.Y. Li, S.Z. Zhao, J.G. Wang, C. Chu, C.L. Li, Promotional mechanisms of activity and SO_2 tolerance of Co- or Ni-doped MnO_x-CeO_2 catalysts for SCR of NO_x with NH_3 at low temperature, Chem. Eng. J. 317 (2017) 20–31, https://doi.org/10.1016/j.cej.2017.02.042.

[39] D.A. Vinnik, A.Yu. Starikov, V.E. Zhivulin, K.A. Astapovich, V.A. Turchenko, T.I. Zubar, S.V. Trukhanov, J. Kohout, T. Kmječ, O. Yakovenko, L. Matzui, A.S.B. Sombra, D. Zhou, R.B. Jotania, C. Singh, A.V. Trukhanov, Structure and magnetodielectric properties of titanium substituted barium hexaferrites, Ceram. Int. 47 (2021) 17293–17306. https://doi.org/10.1016/j.ceramint.2021.03.041.

[40] X. Gao, Y. Jiang, Y.C. Fu, Y. Zhong, Z.Y. Luo, K.F. Cen, Preparation and characterization of CeO_2/TiO_2 catalysts for selective catalytic reduction of NO with NH_3, Catal. Commun. 11 (2010) 465–469, https://doi.org/10.1016/j.catcom.2009.11.024.

[41] L. Zhang, L.L. Li, Y. Cao, X.J. Yao, C.Y. Ge, F. Gao, Y. Deng, C.J. Tang, L. Dong, Getting insight into the influence of SO_2 on TiO_2/CeO_2 for the selective catalytic reduction of NO by NH_3, Appl. Catal. B Environ. 165 (2015) 589–598, https://doi.org/10.1016/j.catcom.2009.11.024.

[42] Y. Jiang, Z.M. Xing, X.C. Wang, S.B. Huang, Q.Y. Liu, J.S. Yang, MoO_3 modified CeO_2/TiO_2 catalyst prepared by a single step sol-gel method for selective catalytic reduction of NO with NH_3, J. Ind. Eng. Chem. 29 (2015) 43–47, https://doi.org/10.1016/j.jiec.2015.04.023.

[43] X. Gao, X.S. Du, L.W. Cui, Y.C. Fu, Z.Y. Luo, K.F. Cen, A Ce-Cu-Ti oxide catalyst for the selective catalytic reduction of NO with NH_3, Catal. Commun. 12 (2010) 255–258, https://doi.org/10.1016/j.catcom.2010.09.029.

[44] L.L. Li, P.X. Li, W. Tan, K.L. Ma, W.X. Zou, C.J. Tang, L. Dong, Enhanced low-temperature NH_3-SCR performance of $CeTiO_x$ catalyst via surface Mo modification, Chinese J. Catal. 41 (2020) 364–373, https://doi.org/10.1016/S1872-2067(19)63437-6.

[45] X.S. Leng, Z.P. Zhang, Y.S. Li, T.R. Zhang, S.B. Ma, F.L. Yuan, X.Y. Niu, Y.J. Zhu, Excellent low temperature NH_3-SCR activity over $Mn_aCe_{0.3}TiO_x$ (a = 0.1-0.3) oxides: Influence of Mn addition, Fuel Process. Technol. 181 (2018) 33–43, https://doi.org/10.1016/j.fuproc.2018.09.012.

[46] Y. Jiang, Z.M. Xing, X.C. Wang, S.B. Huang, X.W. Wang, Q.Y. Liu, Activity and characterization of a Ce-W-Ti oxide catalyst prepared by a single step sol–gel method for selective catalytic reduction of NO with NH_3, Fuel. 151 (2015) 124–129, https://doi.org/10.1016/j.fuel.2015.01.061.

[47] A.L. Kozlovskiy, A. Alina, M.V. Zdorovets, Study of the effect of ion irradiation on increasing the photocatalytic activity of WO_3 microparticles, J. Mater. Sci.: Mater. Electron. 32 (2021) 3863−3877, https://doi.org/10.1007/s10854-020-05130-8.

[48] D.I. Tishkevich, T.I. Zubar, A.L. Zhaludkevich, I.U. Razanau, T.N. Vershinina, A.A. Bondaruk, E.K. Zheleznova, M. Dong, M.Y. Hanfi, M.I. Sayyed, M.V. Silibin, S.V. Trukhanov, A.V. Trukhanov, Isostatic

589 hot pressed W-Cu composites with nanosized grain boundaries: microstructure, structure, and radiation
590 shielding efficiency against gamma-rays, Nanomaterials 12 (2022) 1642,
591 https://doi.org/10.3390/nano12101642.
592 [49] W.P. Shan, F.D. Liu, H. He, X.Y. Shi, C.B. Zhang, A superior Ce-W-Ti mixed oxide catalyst for the selective
593 catalytic reduction of NO_x with NH_3, Appl. Catal. B Environ. 115–116 (2012) 100–106,
594 https://doi.org/10.1016/j.apcatb.2011.12.019.
595 [50] G. Park, M. Kim, J. Cha, H. Kim, H. Lee, Local atomic structure and enhanced catalytic activity of W doped
596 $CeWTiO_x$ catalysts, J. Solid State Chem. 292 (2020) 121689, https://doi.org/10.1016/j.jssc.2020.121689.
597 [51] S.R. Yousefi, D. Ghanbari, M. Salavati-Niasari, Hydrothermal Synthesis of Nickel Hydroxide Nanostructures
598 and Flame Retardant Poly Vinyl Alcohol and Cellulose Acetate Nanocomposites, J. Nanostruct. 6 (2016)
599 77–82, https://doi.org/10.7508/jns.2016.01.00*.
600 [52] S.V. Trukhanov, A.V. Trukhanov, V.A. Turchenko, An.V. Trukhanov, E.L. Trukhanova, D.I. Tishkevich,
601 V.M. Ivanov, T.I. Zubar, M. Salem, V.G. Kostishyn, L.V. Panina, D.A. Vinnik, S.A. Gudkova, Polarization
602 origin and iron positions in indium doped barium hexaferrites, Ceram. Int. 44 (2018) 290 – 300.
603 https://doi.org/10.1016/j.ceramint.2017.09.172.
604 [53] A.L. Kozlovskiy, M.V. Zdorovets, Synthesis, structural, strength and corrosion properties of thin films of the
605 type CuX (X = Bi, Mg, Ni), J. Mater. Sci.: Mater. Electron. 30 (2019) 11819–11832.
606 https://doi.org/10.1007/s10854-019-01556-x.
607 [54] T.I. Zubar, S.A. Sharko, D.I. Tishkevich, N.N. Kovaleva, D.A. Vinnik, S.A. Gudkova, E.L. Trukhanova, E.A.
608 Trofimov, S.A. Chizhik, L.V. Panina, S.V. Trukhanov, A.V. Trukhanov, Anomalies in Ni-Fe nanogranular
609 films growth, J. Alloys Compd. 748 (2018) 970–978. https://doi.org/10.1016/j.jallcom.2018.03.245.
610 [55] J. Yao, Z.P. Zhong, TiO_2 preparation by improved homogeneous precipitation and application in SCR catalyst,

611 J. Cent. South Univ. 23 (2016) 2139−2145, https://doi.org/10.1007/s11771-016-3270-2.

612 [56] J. Liu, Z.B. Xiong, F. Zhou, W. Lu, J. Jin, S.F. Ding, Promotional effect of H_2O_2 modification on the

613 cerium-tungsten-titanium mixed oxide catalyst for selective catalytic reduction of NO with NH_3, J. Phys. Chem.

614 Solids. 121 (2018) 360–366, https://doi.org/10.1016/j.jpcs.2018.05.051.

615 [57] M.A. Mahdi, S.R. Yousefi, L.S. Jasim, M. Salavati-Niasari, Green synthesis of $DyBa_2Fe_3O_{7.988}$/$DyFeO_3$

616 nanocomposites using almond extract with dual eco-friendly applications: Photocatalytic and antibacterial

617 activities, Int. J. Hydrogen Energ. 47 (2022) 14319–14330,

618 https://www.sid.ir/en/journal/ViewPaper.aspx?id=506268.

619 [58] X.S. Liu, Q.F. Yu, H.F. Chen, P. Jiang, J.F. Li, Z.Y. Shen, The promoting effect of S-doping on the NH_3-SCR

620 performance of MnO_x/TiO_2 catalyst, Appl Surf Sci. 508 (2020) 144694,

621 https://doi.org/10.1016/j.apsusc.2019.144694.

622 [59] S.R. Yousefi, A. Sobhani, M. Salavati-Niasari, A new nanocomposite superionic system ($CdHgI_4/HgI_2$):

623 Synthesis, characterization and experimental investigation, Adv. Powder. Technol. 28 (2017) 1258–1262,

624 https://doi.org/10.1016/j.apt.2017.02.013.

625 [60] R. Zhang, Q. Zhong, W. Zhao, L.M. Yu, H.X. Qu, Promotional effect of fluorine on the selective catalytic

626 reduction of NO with NH_3 over CeO_2-TiO_2 catalyst at low temperature, Appl Surf Sci. 289 (2014) 237–244,

627 https://doi.org/10.1016/j.apsusc.2013.10.143.

628 [61] Y.Q. Zeng, Y.N. Wang, P. Hongmanorom, Z.G. Wang, S.L. Zhang, J.T. Chen, Q. Zhong, S. Kawi, Active sites

629 adjustable phosphorus promoted CeO_2/TiO_2 catalysts for selective catalytic reduction of NO_x by NH_3, Chem.

630 Eng. J. 409 (2021) 128242, https://doi.org/10.1016/j.cej.2020.128242.

631 [62] C.X. Liu, L. Chen, J.H. Li, L. Ma, H. Arandiyan, Y. Du, J.Y. Xu, J.M. Hao, Enhancement of Activity and Sulfur

632 Resistance of CeO_2 Supported on TiO_2–SiO_2 for the Selective Catalytic Reduction of NO by NH_3, Environ. Sci.

633 Technol. 46 (2012) 6182–6189, https://doi.org/10.1021/es3001773.

634 [63] Q.L. Cong, L. Chen, X.X. Wang, H.Y. Ma, J.K. Zhao, S.J. Li, Y. Hou, W. Li, Promotional effect of

635 nitrogen-doping on a ceria unary oxide catalyst with rich oxygen vacancies for selective catalytic reduction of

636 NO with NH_3, Chem. Eng. J. 379 (2020) 122302, https://doi.org/10.1016/j.cej.2019.122302.

637 [64] H. Zeng, M. Wu, H.Q. Wang, J.C. Zheng, J.Y. Kang, Tuning the magnetic and electronic properties of

638 strontium titanate by carbon doping, Front. Phys-Beijing. 16 (2021) 43501,

639 https://doi.org/10.1007/s11467-020-1034-9.

640 [65] S.R. Yousefi, D. Ghanbari, M. Salavati-Niasari, M. Hassanpour, Photo-degradation of organic dyes: simple

641 chemical synthesis of $Ni(OH)_2$ nanoparticles, $Ni/Ni(OH)_2$ and Ni/NiO magnetic nanocomposites, J. Mater

642 Sci-Mater. EI. 27 (2016) 1244–1253, https://doi.org/10.1007/s10854-015-3882-6.

643 [66] Jigyasa, J.K. Rajput, Bio-polyphenols promoted green synthesis of silver nanoparticles for facile and

644 ultra-sensitive colorimetric detection of melamine in milk, Biosens. Bioelectron. 120 (2018) 153–159,

645 https://doi.org/10.1016/j.bios.2018.08.054.

646 [67] G.L. Wang, H.J. Jiao, X.Y. Zhu, Y.M. Dong, Z.J. Li, Enhanced fluorescence sensing of melamine based on

647 thioglycolic acid-capped CdS quantum dots, Talanta. 93 (2012) 398–403,

648 https://doi.org/10.1016/j.talanta.2012.02.062.

649 [68] W. Wang, M.O. Tadé, Z.P. Shao, Nitrogen-doped simple and complex oxides for photocatalysis: A review,

650 Prog. Mater. Sci. 92 (2018) 33–63, https://doi.org/10.1016/j.pmatsci.2017.09.002.

651 [69] R. Asahi, T. Morikawa, T. Ohwaki, K. Aoki, Y. Taga, Visible-Light Photocatalysis in Nitrogen-Doped

652 Titanium Oxides, Science. 293 (2001) 269–271, https://doi.org/10.1126/science.1061051.

653 [70] J.P. Wang, B.B. Huang, Z.Y. Wang, X.Y. Qin, X.Y. Zhang, Synthesis and characterization of C, N-codoped

654 TiO_2 nanotubes/nanorods with visible-light activity, Rare Met. 30 (2011) 161–165,

https://doi.org/10.1007/s12598-011-0261-1.

[71] L. Yao, Q.C. Liu, S. Mossin, D. Nielsen, M. Kong, L.J. Jiang, J. Yang, S. Ren, J. Wen, Promotional effects of nitrogen doping on catalytic performance over manganese-containing semi-coke catalysts for the NH_3-SCR at low temperatures, J. Hazard. Mater. 387 (2020) 121704, https://doi.org/10.1016/j.jhazmat.2019.121704.

[72] H.L. Huang, W.P. Shan, S.J. Yang, J.H. Zhang, Novel approach for a cerium-based highly-efficient catalyst with excellent NH_3-SCR performance, Catal. Sci. Technol. 4 (2014) 3611–3614, https://doi.org/10.1039/C4CY00926F.

[73] Q.H. Liang, B.B. Shao, S.H. Tong, Z.F. Liu, L. Tang, Y. Liu, M. Cheng, Q.Y. He, T. Wu, Y. Pan, J. Huang, Z. Peng, Recent advances of melamine self-assembled graphitic carbon nitride-based materials: Design, synthesis and application in energy and environment, Chem. Eng. J. 405 (2021) 126951, https://doi.org/10.1016/j.cej.2020.126951.

[74] Z. Mo, H. Xu, Z.G. Chen, X.J. She, Y.H. Song, P.C. Yan, L. Xu, Y.C. Lei, S.Q. Yuan, H.M. Li, Self-assembled synthesis of defect-engineered graphitic carbon nitride nanotubes for efficient conversion of solar energy, Appl. Catal. B Environ. 225 (2018) 154–161, https://doi.org/10.1016/j.apcatb.2017.11.041.

[75] X. Sun, R.T. Guo, S.W. Liu, J. Liu, W.G. Pan, X. Shi, H. Qin, Z.Y. Wang, Z.Z. Qiu, X.Y. Liu, The promoted performance of CeO_2 catalyst for NH_3-SCR reaction by NH_3 treatment, Appl Surf Sci. 462 (2018) 187–193, https://doi.org/10.1016/j.apsusc.2018.08.114.

[76] Q. Huang, K. Wei, H.D. Xia, Investigations in the recrystallization of evolved gases from pyrolysis process of melamine. J. Therm. Anal. Calorim. 138 (2019) 3897–3903. https://doi.org/10.1007/s10973-019-08338-x.

[77] J.Z. Chen, L.Y. Guo, H.C. Zhu, Y. Qiu, D.J. Yin, T. Zhang, J.J. Chen, Y. Peng, J.H. Li, Balancing redox and acidic properties for optimizing catalytic performance of SCR catalysts: A case study of nanopolyhedron CeO_x-supported WO_x, J. Environ. Chem. Eng. 9 (2021) 105828, https://doi.org/10.1016/j.jece.2021.105828.

[78] X.L. Tang, C.Z. Wang, F.Y. Gao, Y.L. Ma, H.H. Yi, S.Z. Zhao, Y.S. Zhou, Effect of hierarchical element doping on the low-temperature activity of manganese-based catalysts for NH_3-SCR, J. Environ. Chem. Eng. 8 (2020) 104399, https://doi.org/10.1016/j.jece.2020.104399.

[79] H. Li, Y.B. Hao, H.Q. Lu, L.P. Liang, Y.Y. Wang, J.H. Qiu, X.C. Shi, Y. Wang, J.F. Yao, A systematic study on visible-light N-doped TiO_2 photocatalyst obtained from ethylenediamine by sol-gel method, Appl Surf Sci. 344 (2015) 112–118, https://doi.org/10.1016/j.apsusc.2015.03.071.

[80] X. Nie, G.Y. Li, P.K. Wong, H.J. Zhao, T.C. An, Synthesis and characterization of N-doped carbonaceous/TiO_2 composite photoanodes for visible-light photoelectrocatalytic inactivation of Escherichia coli K-12, Catal. Today. 230 (2014) 67–73, https://doi.org/10.1016/j.cattod.2013.09.046.

[81] S.V. Trukhanov, V.A. Khomchenko, L.S. Lobanovski, M.V. Bushinsky, D.V. Karpinsky, V.V. Fedotova, I.O. Troyanchuk, A.V. Trukhanov, S.G. Stepin, R. Szymczak, C.E. Botez, A. Adair, Crystal structure and magnetic properties of Ba-ordered manganites $Ln_{0.70}Ba_{0.30}MnO_{3-\delta}$ (Ln = Pr, Nd), J. Exp. Theor. Phys. 103 (2006) 398–410, https://doi.org/10.1134/S1063776106090093.

[82] A.L. Kozlovskiy, D.I. Shlimas, M.V. Zdorovets, Synthesis, structural properties and shielding efficiency of glasses based on TeO_2-(1-x)ZnO-xSm_2O_3, J. Mater. Sci.: Mater. Electron. 32 (2021) 12111–12120, https://doi.org/10.1007/s10854-021-05839-0.

[83] W.W. Xie, G.D. Zhang, B. Mu, Z.C. Tang, J.Y. Zhang, The promoting effect of palygorskite on CeO_2-WO_3-TiO_2 catalyst for the selective catalytic reduction of NO_x with NH_3, Appl. Clay Sci. 192 (2020) 105641, https://doi.org/10.1016/j.clay.2020.105641.

[84] W.P. Shan, F.D. Liu, H. He, X.Y. Shi, C.B. Zhang, Novel cerium-tungsten mixed oxide catalyst for the selective catalytic reduction of NO_x with NH_3, Chem. Commun. 47 (2011) 8046–8048, https://doi.org/10.1039/c1cc12168e.

699 [85] Y.Q. Li, P. Jiang, J.Q. Tian, Y. Liu, Y.J. Wan, K. Zhang, D.H. Wang, J.M. Dan, B. Dai, X.L. Wang, F. Yu,
700 3D-printed monolithic catalyst of Mn-Ce-Fe/attapulgite for selective catalytic reduction of nitric oxide with
701 ammonia at low temperature, J. Environ. Chem. Eng. 9 (2021) 105753,
702 https://doi.org/10.1016/j.jece.2021.105753.
703 [86] L.Y. Zong, G.D. Zhang, H.J. Zhao, J.Y. Zhang, Z.C. Tang, One pot synthesized CeO_2-WO_3-TiO_2 catalysts with
704 enriched TiO_2 (0 0 1) facets for selective catalytic reduction of NO with NH_3 by evaporation-induced
705 self-assembly method, Chem. Eng. J. 354 (2018) 295–303, https://doi.org/10.1016/j.cej.2018.07.199.
706 [87] I.O. Troyanchuk, S.V. Trukhanov, D.D. Khalyavin, H. Szymczak, Magnetic properties of anion deficit
707 manganites $Ln_{0.55}Ba_{0.45}MnO_{3-\gamma}$ (Ln=La, Nd, Sm, Gd, $\gamma \leqslant 0.37$), J. Magn. Magn. Mater. 208 (2000) 217–220,
708 https://doi.org/10.1016/S0304-8853(99)00529-6.
709 [88] A. Kozlovskiy, K. Egizbek, M.V. Zdorovets, M. Ibragimova, A. Shumskaya, A.A. Rogachev, Z.V. Ignatovich,
710 K. Kadyrzhanov, Evaluation of the efficiency of detection and capture of manganese in aqueous solutions of
711 $FeCeO_x$ nanocomposites doped with Nb_2O_5, Sensors 20 (2020) 4851, https://doi.org/10.3390/s20174851.
712 [89] C. Gao, J.W. Shi, Z.Y. Fan, Y.K. Yu, J.S. Chen, Z.H. Li, C.M. Niu, Eu-Mn-Ti mixed oxides for the SCR of NO_x
713 with NH_3: The effects of Eu-modification on catalytic performance and mechanism, Fuel Process. Technol. 167
714 (2017) 322–333, https://doi.org/10.1016/j.fuproc.2017.07.006.
715 [90] F.X. Li, X.D. Xiao, C. Zhao, J.N. Liu, Q. Li, C.Y. Guo, C.G. Tian, L.P. Zhang, J.A. Hu, B.J. Jiang,
716 TiO_2-on-C_3N_4 double-shell microtubes: In-situ fabricated heterostructures toward enhanced photocatalytic
717 hydrogen evolution, J. Colloid Interface Sci. 572 (2020) 22–30, https://doi.org/10.1016/j.jcis.2020.03.071.
718 [91] S.F. Sun, M.X. Sun, Y.L. Fang, Y. Wang, H.P. Wang, One-step in situ calcination synthesis of g-C_3N_4 /N-TiO_2
719 hybrids with enhanced photoactivity, RSC Adv. 6 (2016) 13063–13071, https://doi.org/10.1039/C5RA26700E.
720 [92] H.Y. Li, S.L. Zhang, Q. Zhong, Effect of nitrogen doping on oxygen vacancies of titanium dioxide supported

721 vanadium pentoxide for ammonia-SCR reaction at low temperature, J. Colloid Interface Sci. 402 (2013)
722 190–195, https://doi.org/10.1016/j.jcis.2012.10.033.
723 [93] X.D. Wang, K. Zhang, X.L. Guo, G.D. Shen, J.Y. Xiang, Synthesis and characterization of N-doped TiO_2
724 loaded onto activated carbon fiber with enhanced visible-light photocatalytic activity, New J. Chem. 38 (2014)
725 6139–6146, https://doi.org/10.1039/c4nj00962b.
726 [94] G.D. Yang, Z. Jiang, H.H. Shi, T.C. Xiao, Z.F. Yan, Preparation of highly visible-light active N-doped TiO_2
727 photocatalyst †, J. Mater. Chem. 20 (2010) 5301–5309, https://doi.org/10.1039/c0jm00376j.
728 [95] K. Wang, Q. Li, B.S. Liu, B. Cheng, W.K. Ho, J.G. Yu, Sulfur-doped g-C_3N_4 with enhanced photocatalytic
729 CO_2-reduction performance, Appl. Catal. B Environ. 176–177 (2015) 44–52,
730 https://doi.org/10.1016/j.apcatb.2015.03.045.
731 [96] H. Liu, Z.Z. Xu, Z. Zhang, D. Ao, Highly efficient photocatalytic H_2 evolution from water over
732 $CdLa_2S_4$/mesoporous g-C_3N_4 hybrids under visible light irradiation, Appl. Catal. B Environ. 192 (2016)
733 234–241, https://doi.org/10.1016/j.apcatb.2016.03.074.
734 [97] J. Arfaouia, A. Ghorbela, C. Petittob, G. Delahay, Effect of acidic components (SO_4^{2-} and WO_3) on the
735 surface acidity, redox ability and NH_3-SCR activity of new CeO_2-TiO_2 nanoporous aerogel catalysts: A
736 comparative study, Inorg. Chem. Commun. 140 (2022) 109494.
737 https://doi.org/10.1016/j.inoche.2022.109494.
738 [98] S.S. Liu, H. Wang, Y. Wei, R.D. Zhang, Core-shell structure effect on CeO_2 and TiO_2 supported WO_3 for the
739 NH_3-SCR process, Mol. Catal. 485 (2020) 110822, https://doi.org/10.1016/j.mcat.2020.110822.
740 [99] Y. Peng, J.H. Li, L. Chen, J.H. Chen, J. Han, H. Zhang, W. Han, Alkali Metal Poisoning of a CeO_2–WO_3
741 Catalyst Used in the Selective Catalytic Reduction of NO_x with NH_3 : an Experimental and Theoretical Study,
742 Environ. Sci. Technol. 46 (2012) 2864–2869, https://doi.org/10.1021/es203619w.

743 [100] L. Chen, D. Weng, J.D. Wang, D. Weng, L. Cao, Low-temperature activity and mechanism of WO_3-modified
744 CeO_2-TiO_2 catalyst under NH_3-NO/NO_2 SCR conditions, Chinese J. Catal. 39 (2018) 1804–1813,
745 https://doi.org/10.1016/S1872-2067(18)63129-8.
746 [101] Q.L. Wang, J.J. Zhou, J.C. Zhang, H. Zhu, Y.H. Feng, J. Jin, Effect of ceria doping on the catalytic activity and
747 SO_2 resistance of MnO_x/TiO_2 catalysts for the selective catalytic reduction of NO with NH_3 at low temperatures,
748 Aerosol Air Qual. Res. 20 (2020) 477–488, https://doi.org/10.4209/aaqr.2019.10.0546.
749 [102] Y. Jiang, G. Cheng, R.N. Yang, H.F. Liu, M. Sun, L. Yu, Z.F. Hao, Influence of Preparation Temperature
750 and Acid Treatment on the Catalytic Activity of MnO_2, J. Solid State Chem. 272 (2019) 173-181,
751 https://doi.org/10.1016/j.jssc.2019.01.031.